

Investigating Impact of Flow Rate and Wettability on Residual Trapping in CO₂ Storage in Saline Aquifers through Relative Permeability Experiments

Mansour Soroush¹, Dag Wessel-Berg², Ole Torsaeter¹ & Jon Kleppe¹

¹ Norwegian University of Science and Technology- NTNU, Trondheim, Norway

² SINTEF, NO-7465, Trondheim, Norway

Correspondence: Mansour Soroush, Department of Petroleum Engineering and Applied Geophysics, NTNU, Trondheim, Norway. Tel: 47-7359-6840. E-mail: mansour.soroush@ntnu.no

Received: April 8, 2013 Accepted: July 31, 2013 Online Published: October 21, 2013

doi:10.5539/eer.v3n2p53

URL: <http://dx.doi.org/10.5539/eer.v3n2p53>

Abstract

In order to investigate effects of injection rate and aquifer influx in imbibition processes and also wettability behaviour for CO₂ storage in aquifers, two representative fluids are chosen for relative permeability measurements. These two fluids represent CO₂ and brine at the reservoir conditions. The first set of experiments is done by n-heptane and a mixture of glycerol and water, flowing in a glass beads porous medium. The density difference and viscosity ratio are designed to be in the range of CO₂-brine systems normally found at reservoir conditions. Another set of experiments is designed based on dodecane and a mixture of glycerol and water. The second mixture is chosen so that the same ratios of density differences and viscosity ratios are maintained. Interfacial tension and contact angles are measured for both cases. By this set up, two cases of strongly water-wet and water-wet systems are designed. The purpose of this study is to quantify the impact of wettability and flow rate through relative permeability experiments. Results show that the relative permeability is sensitive to both rate and wettability, and after interpreting the data from experiments in a history matching process, based on the effects of drainage and imbibition rates and also the effect of wettability, correlations are developed to predict the amount of CO₂ trapped in the pores. This newly developed method will be useful in obtaining good estimations of real case trapping volume in CO₂ storage processes. Scaling analysis of the experiment shows that the tests are well designed in the range of real reservoir conditions.

Keywords: CO₂ storage, residual trapping, relative permeability, imbibition, drainage, CO₂-brine systems, hysteresis, wettability, rate, history matching, scaling

Nomenclature

d Glass beads diameter, μm

GBs Glass beads

CGR Capillary to gravity ratio

k Absolute permeability, md

k_r Relative permeability

S Saturation, fraction

S_w Water saturation, fraction

S_g Gas (CO₂) saturation, fraction

P_c Capillary pressure, mbar

L, E, T, A and B Constants in k_r models

M Mobility ratio

N Correy parameter

N_c Capillary number

Q flux, m/s

U Characteristics velocity, m/s

φ Porosity, %

ρ Density, gr/cc

α Dipping angle, degree

μ Dynamic viscosity, cP

λ Pore size distribution index

γ Interfacial tension, mN/m

Subscripts

g Gas (CO₂)

w Water

i initial

ir irreducible

r residual

Superscript

0 End point value

* Normalized value

1. Introduction

A good option for reduction of the emission of CO₂ to the atmosphere is CO₂ capture and storage (Bennion & Bachu, 2005). CO₂ storage in geological formations is considered to be an important solution for preventing CO₂ emissions to the atmosphere; however, it is vital to ensure safe and secure storage projects. Success of the project is highly dependent on understanding the process in the reservoirs and different geological characteristics. There are many potential geological storage possibilities including depleted oil and gas reservoirs and coal beds, but the main attraction of brine formations as suitable storage sites for CO₂ is the availability and possibly larger volumes (Bennion & Bachu, 2005).

A successful CO₂ storage project in the aquifers requires accurate modeling of the CO₂ behaviour in the subsurface formation. One of the important issues in the modeling process is the relative permeability (the ability of flow of a fluid through a porous material in presence of other fluid) of the CO₂-brine system. Relative permeabilities of these systems are influenced by different reservoir parameters such as absolute permeability (the ability of flow of a fluid through a porous material), temperature, wettability, hysteresis effect, interfacial tension and displacement rates. Many factors have been targeted for the studies in previous petroleum researches, but not many specific research projects on CO₂-brine systems are reported (Perrin et al., 2009; Pini et al., 2011; Krever et al., 2011).

There are some relative permeability measurements reported for CO₂-brine systems. Bennion et al. (2008) studied the impact of interfacial tension and pore size distribution and capillary pressure on CO₂ relative permeability at reservoir conditions. They did experiments on three sandstone and carbonate samples that are representing potential sequestration zones. They observed that the database of measured relative permeability for different zones allows appropriate selection of CO₂-brine sites. Later, the database has been applied in simulation studies.

Recent investigations of CO₂-brine systems, including experimental capillary pressure and relative permeability studies, have been reported by the Benson research team at Stanford. Perrin et al. (2009) reported two sets of relative permeability measurements at different flooding rates. They have also reported slight difference in the end points and corresponding relative permeability values due to the injection rate. Pini et al. (2011) have reported experiments on capillary pressure and heterogeneity of the CO₂-brine systems in sandstone rocks at reservoir conditions. They have used an experimental configuration in addition to a medical X-ray computer tomography (CT) scanner to determine the saturations. They have also observed the rate dependency in the capillary pressure measurements. Kua et al. (2011) reported simulation studies of the effects of flow rate and small-scale heterogeneities on multiphase flow of CO₂ and brine. They have simulated steady-state core scale multiphase flow experiments at wide range of fractional flows and concluded that when the rates are large enough or low enough gravity effect is minimized. Krever et al. (2011) have measured relative permeability and completed studies on trapping of CO₂ in sandstone rocks at reservoir conditions. They have measured drainage relative permeability and residual gas saturations at reservoir conditions. They have reported that the relative permeability in four samples was consistent with general characteristics of drainage in strongly water-wet rocks. They observed that residual trapping can play a major role in the immobilization of CO₂ injected into the subsurface and they have suggested that further investigations should be performed to establish the wetting properties of rocks. Krause et al. (2011) did laboratory core flooding experiments coupled with CT scanning. They have used the results to measure core properties such as absolute and relative permeability, and also to determine sub-core scale saturation and porosity distributions. In that study by doing experiments on the subcore scale, fluid distributions during the displacement process, displacement efficiency of CO₂-brine drainage processes, residual trapping and fluid saturation at the millimeter to sub-millimeter scale were studied.

The effect of gravitational forces on capillary trapping during CO₂ storage has been studied by Bandara et al. (2011). They have used pore scale models to provide sensitivity analysis of the trapping volume to the gravity number. Their results show that, for instance, for large gravity numbers, most of the injected CO₂ reached to the caprock. Another work by Suekane et al. (2011) also clarifies the effect of gravity through imaging the trapped air bobbles in Berea sandstone after spontaneous imbibition at atmospheric pressure. They reported that trapped N₂ bubbles are stable against the water flow rate corresponding to a capillary number in the range of 1.0×10^{-4} .

There are also some researches in theoretical and analytical aspects of the residual trapping problem. Spiteri et al. (2008) developed a new trapping model based on pore scale modeling. They believe that hysteresis is the most important factor in the prediction of CO₂ trapping.

Wettability and flow rate in both drainage and imbibition processes can affect the residual trapping mechanism and this is quantified through this study. The aim of this study is to target this problem through relative permeability experiments and to find correlations to apply the results in real storage sites. Scaling analysis of the experiment admits that the tests are designed in the range of real reservoir conditions. The correlations give good estimation of the trapped volume based on injection rate and wettability characteristics.

2. Methods

2.1 Relative Permeability Measurement Methods

Steady-state and unsteady-state methods are two procedures for measuring relative permeability. In steady-state method, fixed ratios of two immiscible fluids are injected at the same time into the porous media until saturation and pressure equilibrium. In unsteady-state method one fluid phase is displaced by another immiscible fluid phase (Honarpour et al., 1986). In this study unsteady-state method is used and relative permeabilities are measured from recorded pressure difference and production during drainage and imbibition. Either explicit or implicit methods can be used for calculating the relative permeability from the experiment data. The widely used explicit method is JBN technique (Jonhson et al., 1959). The implicit method uses numerical simulations for history matching (Wang et al., 2006). The history matching of the data in this study is done by Sendra software. In that a two phase one dimensional black oil simulation model is used for interpreting the flooding data. Through this process the experimental data matched by adjusting the relative permeability models. There are different correlations that may be used to match the relative permeability from the experiment data. In the Sendra simulator these correlations are described as follows. The normalized water saturation is used in all correlations:

$$S_w^* = \frac{S_w - S_{wi}}{1 - S_{wi} - S_{gr}} \quad (1)$$

For CO₂-brine systems, the formulations are given for gas-water; but they are similar for oil-water and oil-gas systems (Sendra user guide, 2012). Burdine (1953) introduced the relative permeability values as below:

$$k_{rw} = k_{rw}^0 (S_w^*)^{\frac{2+3\lambda}{\lambda}} \quad (2)$$

$$k_{rg} = k_{rg}^0 (1 - S_w^*)^2 \left[1 - (1 - S_w^*)^{\frac{2+\lambda}{\lambda}} \right] \quad (3)$$

In that, the superscript 0 is the end point value, superscript * is normalized value for water saturation from equation (1) and λ is the pore size distribution index (Burdine, 1953). Later, Corey (1954) proposed a new correlation that has been widely used:

$$k_{rw} = k_{rw}^0 (S_w^*)^{N_w} \quad (4)$$

$$k_{rg} = k_{rg}^0 (1 - S_w^*)^{N_g} \quad (5)$$

N_w and N_g are the water and gas Corey parameters. These parameters define the curvature of water and gas relative permeability plots. Sigmund and McCaffery (1972) modified the Corey correlation:

$$k_{rw} = k_{rw}^0 \frac{(S_w^*)^{N_w + A} S_w^*}{1 + A} \quad (6)$$

$$k_{rg} = k_{rg}^0 \frac{(1 - S_w^*)^{N_g + B} (1 - S_w^*)}{1 + B} \quad (7)$$

Here N_w and N_g are the same as Corey parameters. The constants A and B are small values for linearizing the curves when relative permeability values approach zero. These equations are the same as Corey equation if the constants A and B are zero. Later, Chierici (1984) introduced new correlation:

$$k_{rw} = k_{rw}(S_{gr}) e^{-BR_w^{-M}} \quad (8)$$

$$k_{rg} = k_{rg}(S_{wi}) e^{-AR_w^L} \quad (9)$$

$$R_w(S_w) = \frac{S_w - S_{wi}}{1 - S_{gr} - S_w} \quad (10)$$

Here, instead of normalized water saturation terms, R_w is used (Chierici, 1984). LET Correlation is developed by Lomeland et al. (2005):

$$k_{rw} = k_{rw}^0 \frac{(S_w^*)^{L_w}}{(S_w^*)^{L_w} + E_w (1 - S_w^*)^{T_w}} \quad (11)$$

$$k_{rg} = k_{rg}^0 \frac{(1 - S_w^*)^{L_g}}{(1 - S_w^*)^{L_g} + E_g (S_w^*)^{T_g}} \quad (12)$$

The parameter L describes the shape of the curve in the lower parts, while the parameter T is related to the top of the curve (Sendra user guide, 2012) (Lomeland et al., 2005). In this study, all the above-mentioned correlations have been examined to find the best possible history matching of the experimental data and in most of the cases the best fit was obtained by using the Sigmund and McCaffery correlation.

Relative permeability models are also developed to predict residual values in flowing systems. These models are usually developed empirically and recently are matched through pore scale network modeling. Land (1971) has developed an imbibition relative permeability relation for two and three phases. In that relation he assumed that trapping volume is function of the non-wetting saturation. Land proposed a widely used empirical correlation that is still the base for some modified models (Soroush et al., 2013).

$$S_{gr}^* = \frac{S_{gi}^*}{1 + CS_{gi}^*} \quad (13)$$

$$S_{gr}^* = \frac{S_{gi}^*}{1 + CS_{gi}^*} \quad (14)$$

$$C = \frac{1}{S_{gr}^{*max}} - 1 \quad (15)$$

In the Land correlation, S_{gr}^* is residual saturation, S_{gi}^* is initial saturation and S_{gr}^{*max} is maximum residual saturation. Killough (1976) developed Land's model by introducing an interpolation method to find scanning curves that is an intermediate curve to predict the relative permeability curve and the end points. In this method relative permeability falls between two endpoint saturations. In Killough's method trapped critical saturation for each value of reached saturation S is:

$$S_{gr} = S_{gr}^{max} + \frac{S - S_{gi}}{1 + C(S - S_{gi})} \quad (16)$$

$$C = \frac{1}{S_{gr}^{max} - S_{gi}} - \frac{1}{S_g^{max} - S_{gi}} \quad (17)$$

Kleppe et al. (1997) questioned the validity of applying Land's trapping relationship. The experiments were based on artificial core analysis (Aeroolithe 10), and did not match Land's results. They proposed a correlation based on the maximum residual saturation at the end of complete imbibition:

$$S_{gr} = \frac{S_{gi}}{S_g^{max}} S_{gr}^{max} \quad (18)$$

Carlson (1981) developed a method that produces a scanning curve that is parallel to the imbibition curve. The idea is shifting the imbibition curve horizontally until it intersects the drainage curve (Schlumberger Eclipse technical description, 2012).

2.2 Analytical Description

For the purpose of analytical description of the residual trapping mechanism during CO₂ storage in the saline aquifers, two phenomena are considered; injection of CO₂ into the subsurface formations and the behaviour of the CO₂ after injection. Then, further development of the model is obtained by adding a dip angle to the formation layers.

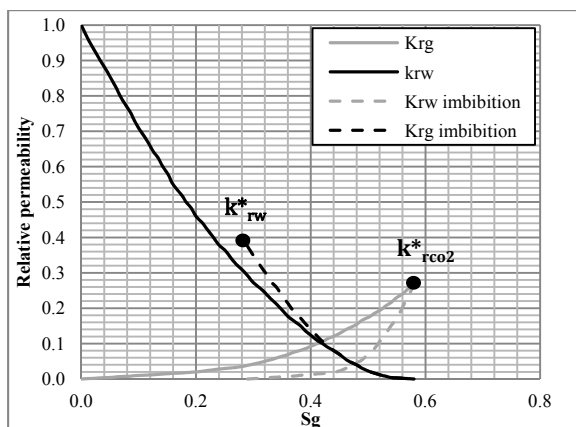


Figure 1. Typical relative permeability curve for CO₂-brine systems, drainage and imbibition

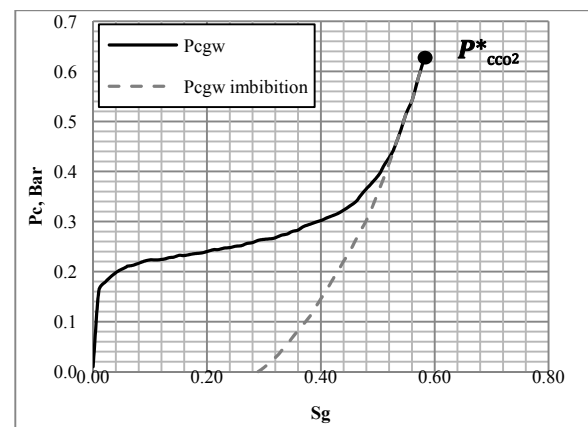


Figure 2. Typical capillary pressure curve for CO₂-brine systems, drainage and imbibition

Here, a one dimensional, two phase system for immiscible and incompressible flow of CO₂ in a narrow porous channel filled with brine has been considered. By introducing dimensionless parameters it is possible to find the scaling parameters for the problem. The medium is initially filled with the brine at $S_w = 1$ and it is designed to be very long compared to the thickness of the reservoir, and it has a dip angle of α . Two typical relative permeability curves with the end point relative permeability values of $k_{rCO_2}^*$, k_{rw}^* and a capillary pressure curve with the maximum pressure of $P_{cCO_2}^*$ are selected for this problem, as shown in Figures 1 and 2 (Soroush et al., 2013). To develop the governing equation, conservation of mass and the Darcy equation have been normalized based on dimensionless length, time, porosity and flux. By simplifying the equation and rearranging, three main dimensionless groups are derived (Soroush et al., 2013). The benefit of this scaling investigation is a relationship between field scale CO₂ storage and experimental results.

$$N_{cv} = \frac{P_c^* k_{rCO_2}^* \bar{k}}{QL\mu_{CO_2}} \quad (19)$$

$$N_{gr} = \frac{\Delta\rho g \sin\alpha k_{rCO_2}^* \bar{k}}{Q\mu_{CO_2}} \quad (20)$$

$$M = \frac{k_{rw}^*/\mu_w}{k_{rCO_2}^*/\mu_{CO_2}} \quad (21)$$

Here, Q is injection flux (m/s) and \bar{k} is average permeability (m²) and L is length of the model (m). Gupta (1979) has introduced the following capillary number for small-scale environment:

$$N_c = \frac{U\mu}{\gamma} \quad (22)$$

Here γ is interfacial tension between two fluids and U is characteristics velocity. The capillary-to-gravity ratio (CGR) has been also defined to provide quantification of the relative effect of gravity in the presence of capillary pressure. CGR definition is first given by Iffly et al. (1997) as follows:

$$N_{gr} = \frac{2\gamma}{\Delta\rho g h \sqrt{\frac{k}{\phi}}} \quad (23)$$

2.3 Experiment Set-Up and Procedure

2.3.1 Fluid Properties

In this study, two sets of fluids are chosen for experiments at laboratory conditions. The fluid selection is based on scaling analysis. This means that density difference and viscosity ratio are chosen in the range of CO₂-brine conditions at the reservoir. The second fluid set has the same scaling ratios but the difference is the wettability behaviour to the porous material. The viscosities of the fluid sets are measured by Brookfield LVDV-II+Pro viscometer, and are measured at atmospheric pressure and 22 °C (Table1). The DV-II+Pro consist of a rotating spindle that is placed in the chamber full of the testing fluid. After calibrating the spring, the viscous drag of the fluid against the spindle is measured by the spring deflection.

Table 1. Fluid properties at laboratory condition

Fluid name	Fluid set 1			Fluid set 2
	n-heptane	glycerol (50%) fresh water (50%)*	dodecane	glycerol (66%) fresh water (34%)*
Molecular formula	C ₇ H ₁₆	C ₃ H ₈ O ₃ +H ₂ O	C ₁₂ H ₂₆	C ₃ H ₈ O ₃ +H ₂ O
Densities (gr/cc)	0.68	1.1	0.78	1.2
Density difference (gr/cc)		0.42		0.42
Viscosities (cp)	0.67	5.8	1.68	14.5
Viscosity ratio ($\frac{\mu_{Hep.}}{\mu_{Gly.+water}}, \frac{\mu_{Dode.}}{\mu_{Gly.+water}}$)		0.1159		0.1155

*based on weight %.

Ranges of fluid properties for the CO₂-brine systems are different for various reservoir conditions but the overall ranges are reported in the literature. CO₂ and brine densities and viscosities are strongly dependent on the

reservoir conditions including depth, temperature and pressure. Salinity of the brine also affects the density and viscosity of it (Nordbotten et al. 2005). Nordbotten et al. (2005) have categorized the reservoir conditions to cold basin with temperature gradient of 25 °C /km, with a surface temperature of around 10 °C, and warm basin with temperature gradient of 45 °C /km, and surface temperature of about 20 °C. Shallow depth is considered to be around 1000 m and deep formations assumed to have around 3000 m depth. Hydrostatic pressure gradient of 10.5 MPa/km is also considered for brine formations. According to these assumptions, Table 2 shows the range of different fluid properties for CO₂-brine systems. Comparing the fluid properties of the designed sets and the typical ranges of density and viscosity of the CO₂ storage sites, good agreement is found between the fluid model designs and deep and cold storage sites.

Table 2. Fluid properties of CO₂ and brine taken from Nordbotten et al. (2005)

	Cold Shallow	Cold Deep	Warm Shallow	Warm Deep
Density of CO ₂ (kg/m³)	714	733	266	479
Density of brine(kg/m³)	1012-1230	995-1202	998-1210	945-1145
Viscosity of CO ₂ (mPa.s)	0.0577	0.0611	0.0395	0.0395
Viscosity of brine (mPa.s)	0.795-1.58	0.378-0.664	0.491-0.883	0.195-0.312
Density difference (kg/m³)	298-516	262-469	732-944	466-666
Viscosity ratio	0.037-0.073	0.095-0.162	0.026-0.127	0.127-0.203

2.3.2 Absolute and Relative Permeability Measurements

Stainless steel chamber is used for having glass beads inside and inserting that in the core holder. The chamber is filled with glass beads through a continuous shaking procedure. After at least one hour of shaking, the glass beads are packed. It is tried to shake the chamber in different directions to have a homogeneous glass beads pattern. Nylon filters (60 μm) in both ends of the chamber prevent glass beads production. The helium porosimeter method has been used for porosity determination. The helium porosimeter utilizes the principle of gas expansion that is described by Boyle's law. To have a known volume of helium gas, the chamber (empty, but with filter papers inside) is filled with helium at a known pressure. Then the helium is expanded into the chamber that is filled with glass beads. The second pressure record depends on the volume of the chamber minus the glass beads volume, so we have the porosity. In the next stage, the chamber is fully saturated with the wetting phase (glycerol mixture with water) by use of vacuum cell. The chamber is placed in the vacuum and after a complete process of vacuuming the mixture opened to the chamber. Figure 3 shows the set up and Figure 4 is the chamber and separator. Schematics of the set-up and connections can be found in Figure 5.

An absolute permeability measurement of the porous media in the chamber is done by injecting a glycerol-water mixture in different rates and recording the pressure drop.

The unsteady-state relative permeability method is used and the chamber is initially filled with a glycerol-water mixture and it is placed into the core holder. n-heptane is vertically injected from the top in the first section of runs (test number 1 to 4 in Table 5) and in the other set of experiments (test numbers 9 to 12 in Table 5) dodecane is injected into the chamber. After a complete drainage (more than 1.2 pore volume injection) imbibition has been performed and the non-wetting phase has been injected into the chamber again vertically from bottom. The test is replicated by injecting glycerol mixtures from each fluid set at the same experimental condition and different injection rates (test number 5 to 8 and 13 to 16 in Table 5).

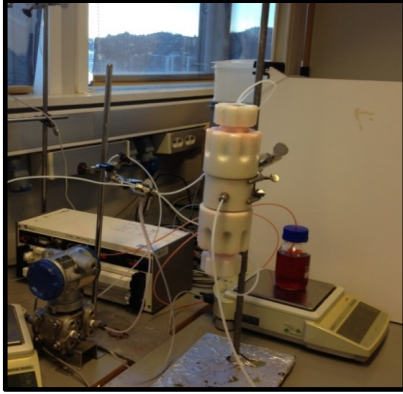


Figure 3. Set-up picture

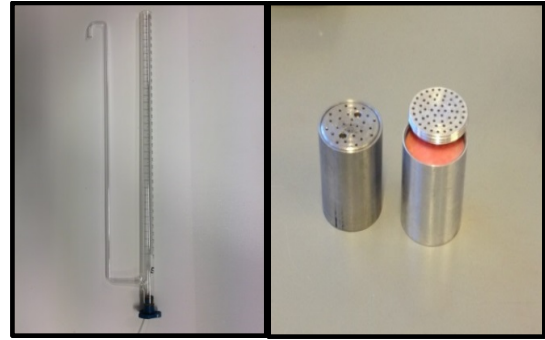


Figure 4. Separator and glass beads chamber

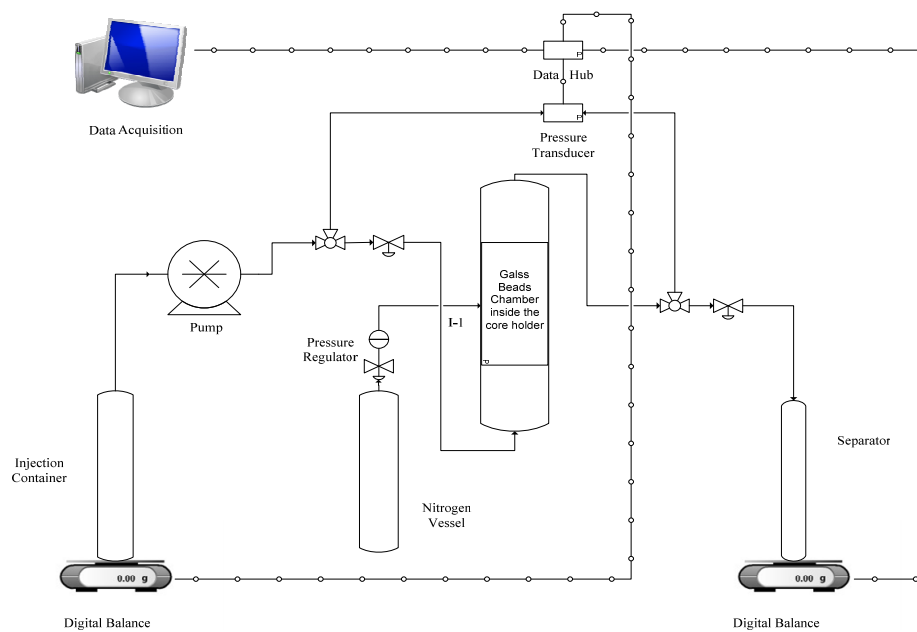


Figure 5. Schematic of the relative permeability set-up

2.3.3 Interfacial Tension (IFT) Measurement

Interfacial tension between two sets of fluids has been measured with pendant drop method. Minimum one hour is considered to let the drop to be stable at atmospheric pressure and 22 °C. Figures 6 and 7 show the droplet after stabilization and the curvature is fitted to obtain the IFT for two sets of the fluids. Figure 8 compares the results of the IFT measurements. Both tests resulted in the same range of IFT and in stabilized period they matched together. The IFT estimations from the experiments are in the range of 26 mN/m . Hebach et al. (2002) studied CO₂-brine IFT at the range of reservoir pressure and reported values is around 30 mN/m . Chiquet et al. (2006) studies also confirmed the former measurement.

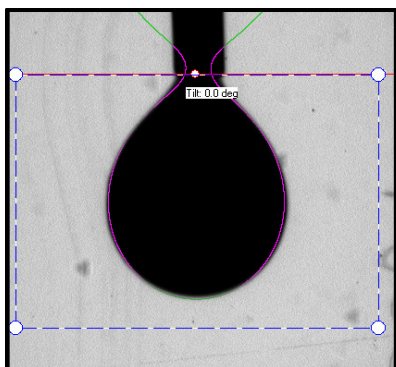


Figure 6. A droplet of heptane in glycerol and water mixture, fluid set 1

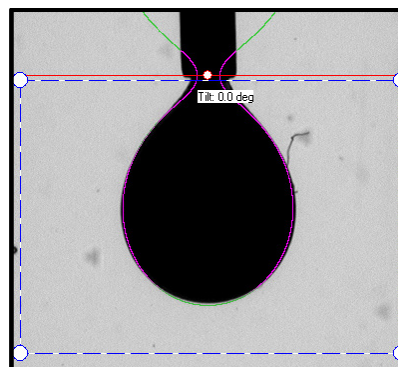


Figure 7. A droplet of dodecane in glycerol and water mixture, fluid set 2

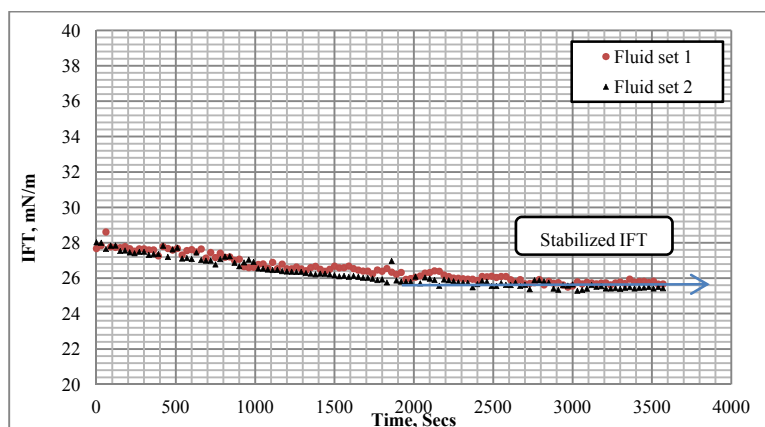


Figure 8. IFT measurement results

2.3.4 Contact Angle Measurements

An imaging method is used for measuring the contact angle for two sets of fluids. Practically, in porous materials it is complex to determine the real contact angle because of the pore shapes and complex mineralogy, but in order to obtain an estimation of the range of contact angle and knowledge about the wetting characteristics of each fluid set, contact angle is measured in presence of fluids and a solid surface of glass that is cleaned and polished. The chamber is filled with the non-wetting phase in each fluid set (n-heptane or dodecane) and a drop of the wetting phase is placed on the glass surface and an enlarged image of the drop is obtained by photography. The experiment continued for minimum one hour to let the droplet to be stable. Very small changes in the angle are observed after one hour of stabilization period. Figures 9 and 10 are droplet photos and matching curves. Figure 11 compares the contact angles obtained from the experiment. Contact angles are calculated for both left and right sides of the drop and almost the same values are predicted, but the final result is the average of right and left measurements. About 16 degrees difference is observed in two experiments. According to conventional wettability criteria wetting phase in fluid set 1 is categorized as strongly wet to the media, while fluid set 2 is considered wet. The wettability characteristic is validated by the result of Amott cell wettability measurements.

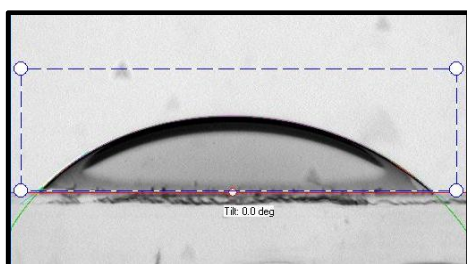


Figure 9. Contact angle measurements, fluid set 1

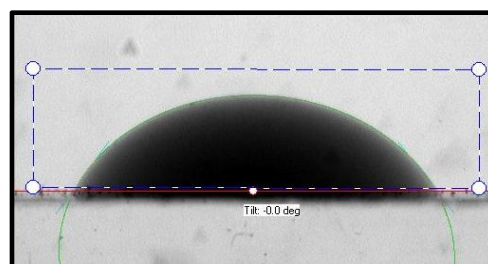


Figure 10. Contact angle measurements, fluid set 2

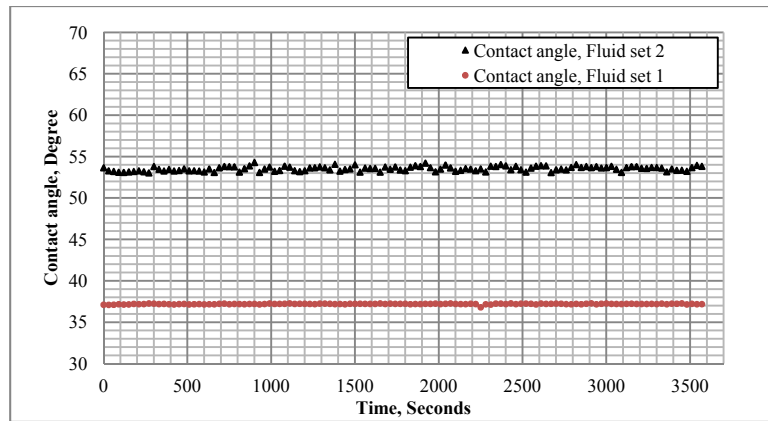


Figure 11. Contact angle measurements for two sets of fluids

2.3.5 Amott Cell Imbibition Test

An Amott cell is used to measure the wettability index of the fluid systems. Only an imbibition process is completed to quantify the residual values of the non-wetting in this test. In this experiment the non-wetting phase will be produced only by the gravitational force and will be accumulated at top of the Amott cell. The chamber that is fully saturated with the non-wetting phase (n-heptane or dodecane) is placed in the imbibition cell surrounded by wetting phase (glycerol and water mixtures). The wetting phase starts to penetrate into the chamber and the non-wetting phase displaces the wetting phase out of the chamber until equilibrium is reached. The mechanism of production can be both spontaneous and gravitational because of having heavier fluid at top of the lighter one in the chamber. The production volume is measured in a scaled section at the top of the cell. The non-wet production gives an estimation of the effect of wettability when repeating the test with fluid set 2 in the same porous condition. As it is shown in Figure 12, production rate is higher in the early stages of the experiment, but it is stabilized at late times.

Table 3. Amott cell experiments design

Test No	fluid	Imbibition test total time, sec	Porosity, %	Distance from top of the chamber to top of the Amott cell, cm	PV, cc	Residual fluid, fraction
1	fluid set 1	30000	39.7	28	15.156	0.173
2	fluid set 2	30000	39.6	28	15.127	0.313

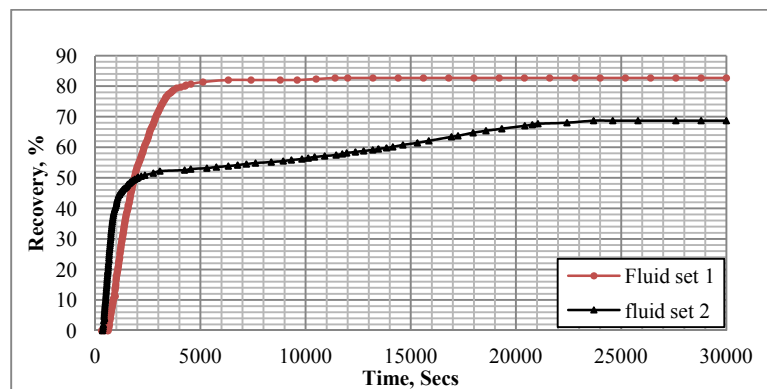


Figure 12. Amott cell imbibition cell results

3. Results

3.1 Absolute Permeability Results

The absolute permeability is used as an adjusting parameter in simulations by the Sendra software to match the experimental pressure drop observed in the relative permeability measurements. The absolute permeability calculation is based on injection of wetting fluid of fluid set 1 by different injection rates. The pressure drop created by the injection is plotted in Figure 13. The stabilized pressure in each step gives a point in the pressure versus rate plot, and by use of the Darcy equation absolute permeability is obtained.

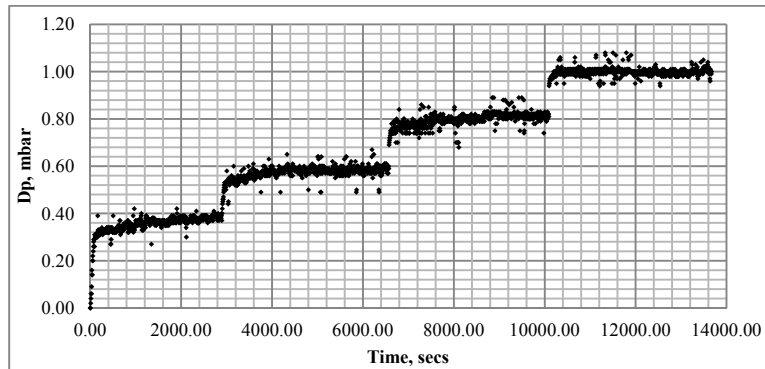


Figure 13. Pressure difference for different rate in injection

Table 4. Stabilized pressure for each injection rate

Rate, cc/min	Rate, cc/sec	Stabilized Dp, mbar	Stabilized Dp, atm
0	0	0	0
0.0667	0.001111	0.37	0.00036519
0.1000	0.001667	0.59	0.00058233
0.1333	0.002222	0.80	0.00078960
0.1667	0.002778	1.00	0.00098700

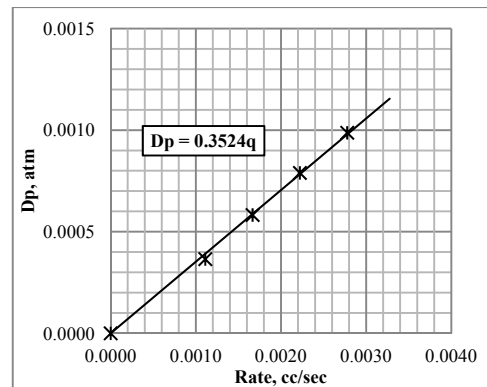


Figure 14. Pressure difference versus injection rate

The results are in good agreement with the correlation given by Rump and Gupta (1975) that is for estimating the absolute permeability in glass bead packs.

$$k = \frac{\phi^{5.5}}{5.6} d^2 \tag{24}$$

Here ϕ is porosity and d is glass bead diameter in μm and permeability will be estimated in md . Table 5 shows experiment condition and table 6 shows the absolute permeability values from experiment and correlation.

Table 5. Experimental conditions

Items	Properties
Injection rate	Variable in each set
System pressure (bar)	Atmospheric pressure
Overburden pressure (bar)	10
Experiment temperature ($^{\circ}\text{C}$)	22
Chamber Length (cm)	5.56
Chamber Diameter (cm)	4.18

Table 6. Absolute permeability measurements

Calculated k, md	Minimum GBs size 70 μm	Maximum GBs size 110 μm	Average
From equation 24	5437	13426	9431
From experiment			7980

3.2 Relative Permeability Results

Table 7 gives overall information about the successful tests done in this study. All the experiments are carried out for porosity of 39.7 % and calculated pore volume is 15.6 cc.

Table 7. Experiments in this study

Experiment type	Test No	Fluids	Injection rate, cc/min	Comments
Drainage	1	fluid set 1	0.1	
	2	fluid set 1	0.2	
	3	fluid set 1	1	
	4	fluid set 1	5	
Imbibition	5	fluid set 1	0.1	
	6	fluid set 1	0.2	
	7	fluid set 1	1	
	8	fluid set 1	5	end points values
Drainage	9	fluid set 2	0.1	
	10	fluid set 2	0.2	
	11	fluid set 2	1	
	12	fluid set 2	5	
Imbibition	13	fluid set 2	0.1	
	14	fluid set 2	0.2	
	15	fluid set 2	1	
	16	fluid set 2	5	end points values

3.2.1 Results for Fluid Set 1

According to the measured absolute permeability and by using history matching of pressure drop and production, the best relative permeability model is matched to the data. Figures 15 and 16 show the history matching results for a very low injection rate test and Figure 17 is a plot of relative permeability obtained from this test. The tests are carried out in different injection rates and the results are presented in Figure 18. Both saturation end-points and corresponding relative permeabilities are affected by the rate. Imbibition tests are completed after the drainage test with the highest rate. Test number 4 is replicated, and afterwards imbibition tests are carried out with different rates. Four different rates of imbibition are examined and three reasonable pressure drops obtained. Very high imbibition rates lead to unstable pressure response but it was still possible to measure the end point values. Figure 21 compares the relative permeability measurements for the imbibition test. The results are less sensitive to the rate, comparing to the drainage tests. Table 8 shows the correlation and parameters used for history matching and end point values. For simplicity, the k_{rg} and k_{rw} terms used in the plots, that are actually relative permeabilities to the non-wetting and wetting phases.

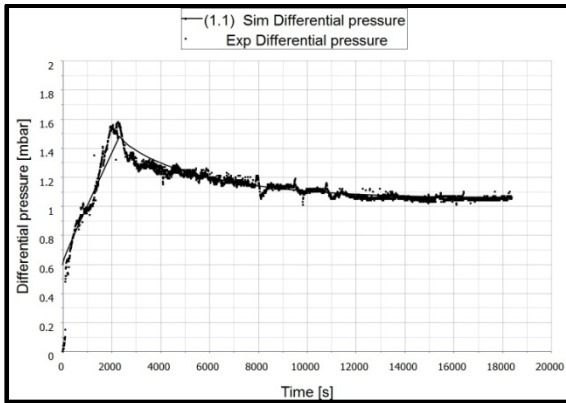


Figure15. Drainage test, history matching of differential pressure, injection rate of 0.1 cc/min

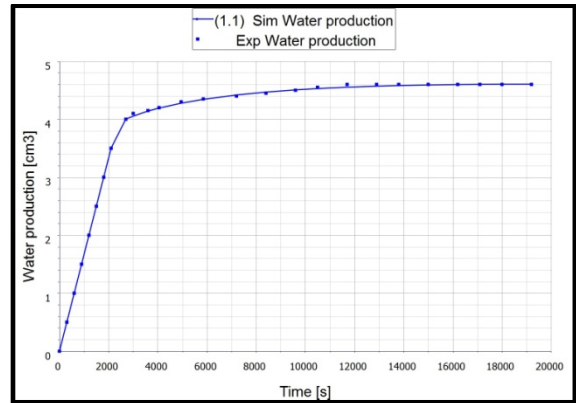


Figure 16. Drainage test, history matching of water production, injection rate of 0.1 cc/min

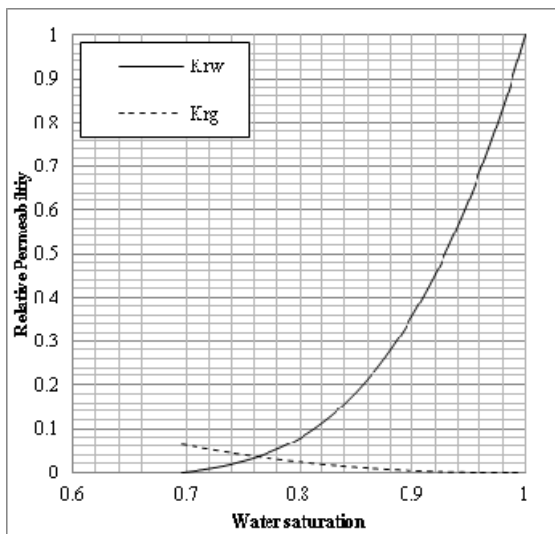


Figure17. Drainage test, injection rate=0.1 cc/min

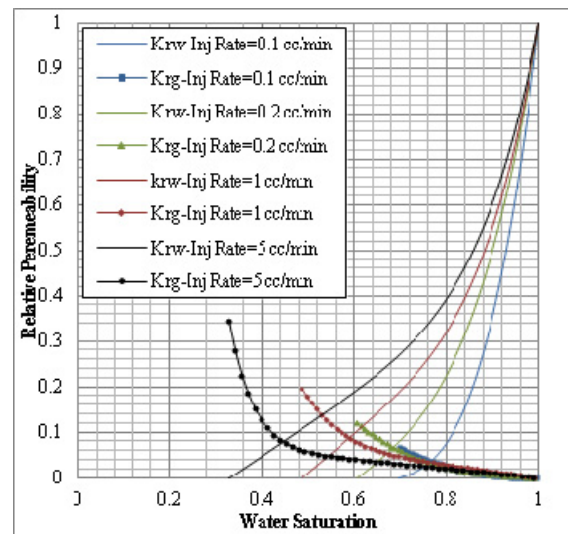


Figure 18. Drainage tests, effect of injection rate

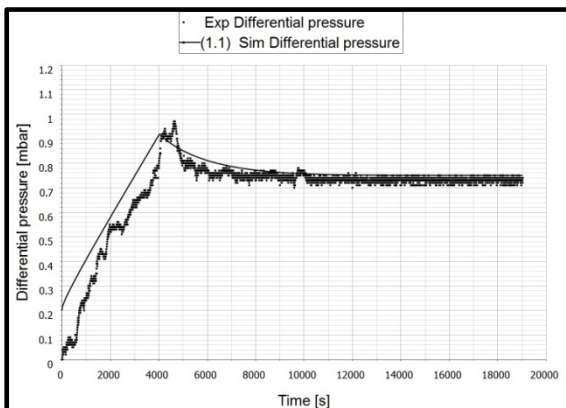


Figure19. Imbibition test, history matching of differential pressure, injection rate of 0.1 cc/min

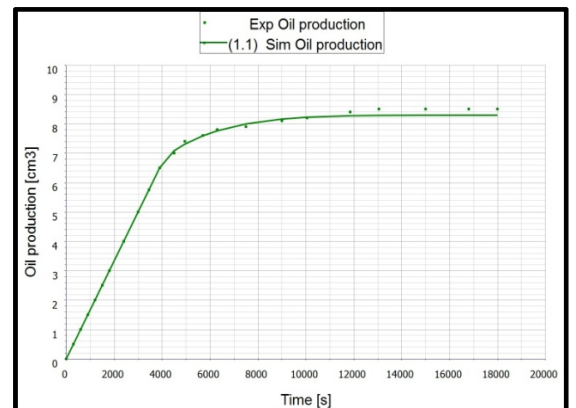


Figure 20. Imbibition test, history matching of water production, injection rate of 0.1 cc/min

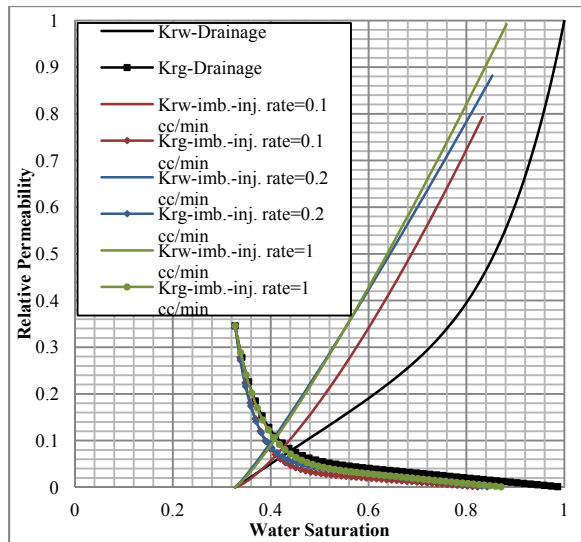


Figure 21. Imbibition tests, effects of injection rate

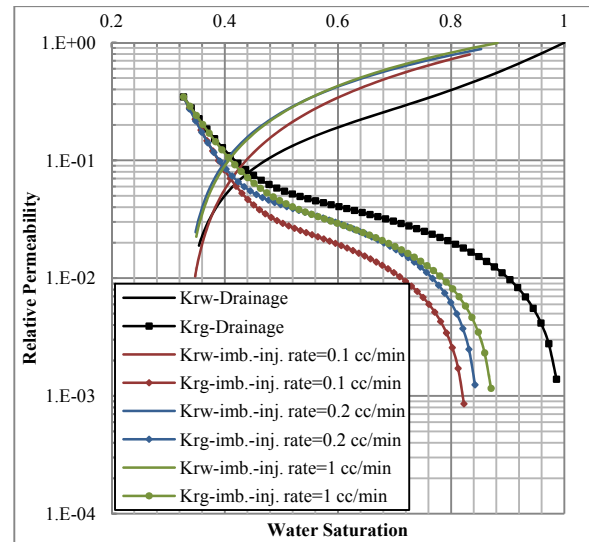


Figure 22. Imbibition tests, effects of injection rate – logarithmic

Table 8. History matching data - fluid set 1

Test type	Correlation	Inj. rate, cc/min	Capillary Number	Nw	Ng	A	B	Krw(Sgi)	Krg(Swir)	Swir	Sgr
Drainage	Sigmund & McCaffery	0.1	1.956×10^{-9}	2.842	2.317	0.116	0.006	1.000	0.065	0.696	0.000
	Sigmund & McCaffery	0.2	3.912×10^{-9}	3.245	3.136	0.479	0.221	1.000	0.121	0.604	0.000
	Sigmund & McCaffery	1	1.956×10^{-8}	4.823	6.631	0.794	0.600	1.000	0.198	0.485	0.000
	Sigmund & McCaffery	5	9.781×10^{-8}	5.765	8.680	0.816	0.245	1.000	0.346	0.327	0.000
Imbibition	Sigmund & McCaffery	0.1	1.693×10^{-7}	1.382	12.110	0.035	0.138	0.793	0.346	0.327	0.167
	Sigmund & McCaffery	0.2	3.867×10^{-7}	1.128	14.188	0.001	0.214	0.882	0.346	0.327	0.147
	Sigmund & McCaffery	1	1.693×10^{-6}	1.184	10.525	0.001	0.197	0.992	0.346	0.327	0.118

3.2.2 Results for Fluid Set 2

The same procedure carried out for fluid set 2. The trend of rate effect is almost the same in the new set of tests but end points and corresponding relative permeabilities are affected due to wettability change. The only variable parameter in this set of experiment is wettability characteristics of the fluids and the porous material. Figures 23 to 28 show the result. Table 9 shows different correlations used to match the results.

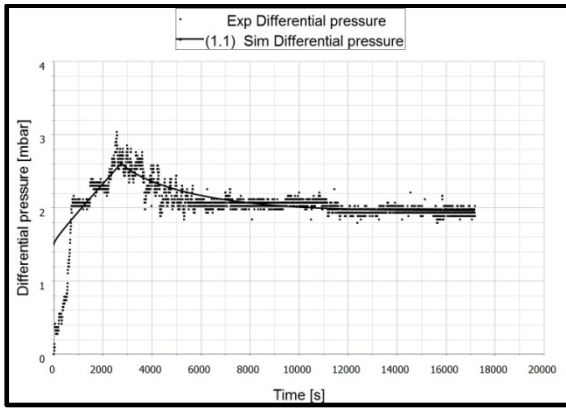


Figure 23. Drainage test, history matching of differential pressure, injection rate=0.1 cc/min

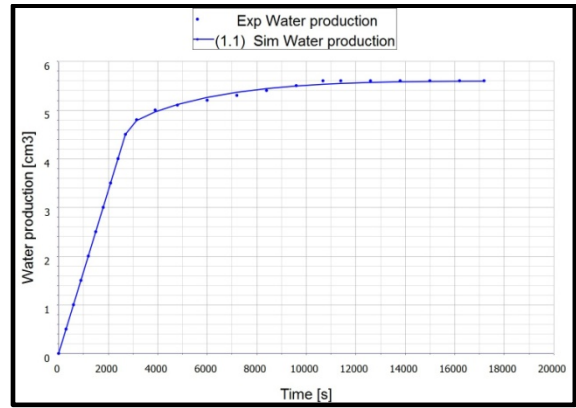


Figure 24. Drainage test, history matching of water production, injection rate=0.1 cc/min

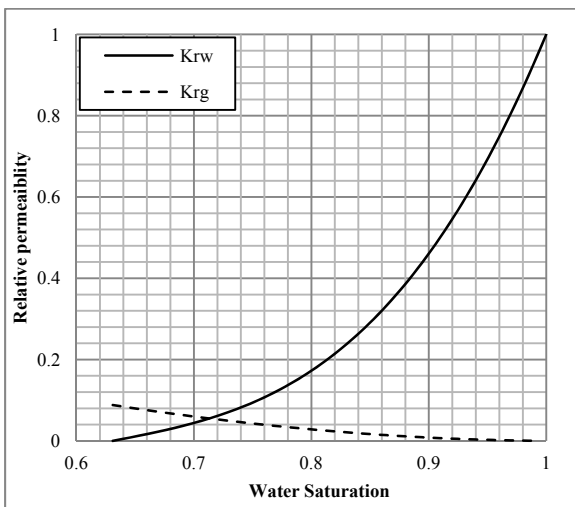


Figure 25. Drainage test, injection rate=0.1 cc/min

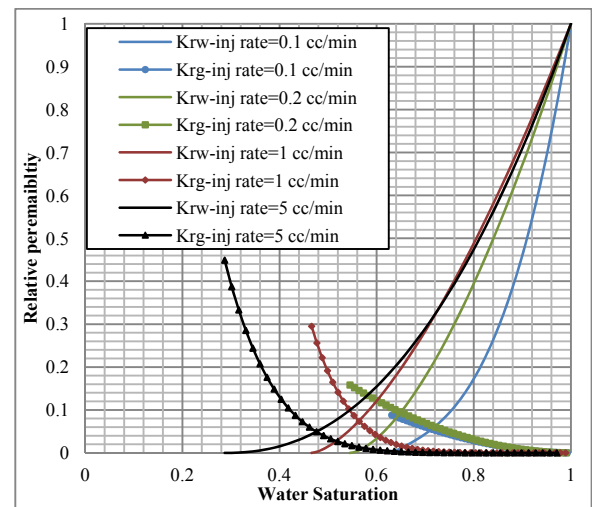


Figure 26. Drainage tests, injection rate=0.1 cc/min

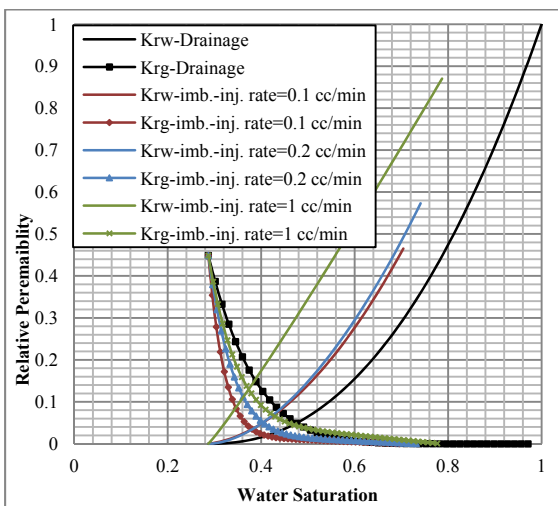


Figure 27. Imbibition tests, effect of injection rate

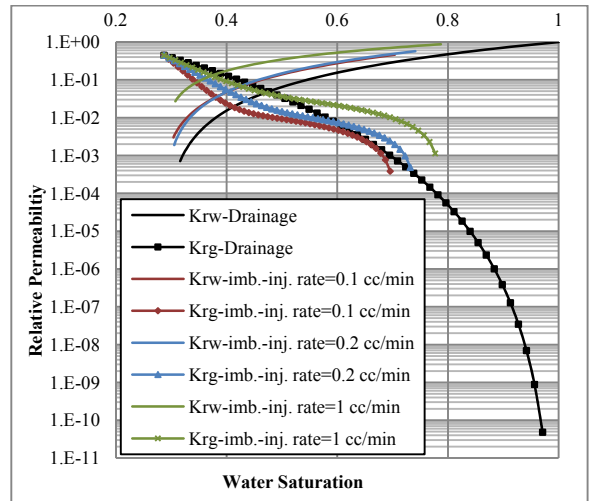


Figure 28. Imbibition tests, effect of injection rate-logarithmic

Table 9. History matching data - fluid set 2

Test type	Correlation	Inj. rate, cc/min	Capillary Number	Nw	Ng	A	B	Krw(Sgi)	Krg(Swir)	Swir	Sgr
Drainage	Sigmund & McCaffery	0.1	4.905×10^{-8}	2.973	1.894	0.260	0.028	1.000	0.088	0.631	0.000
	Sigmund & McCaffery	0.2	9.810×10^{-7}	1.607	1.988	0.001	0.015	1.000	0.158	0.545	0.000
	Sigmund & McCaffery	1	4.905×10^{-7}	1.527	6.852	-	-	1.000	0.295	0.466	0.000
	Sigmund & McCaffery	5	2.454×10^{-6}	2.266	3.542	-	-	1.000	0.449	0.287	0.000
Imbibition	Sigmund & McCaffery	0.1	4.233×10^{-7}	1.928	12.010	0.127	0.044	0.465	0.449	0.287	0.296
	Sigmund & McCaffery	0.2	8.467×10^{-7}	1.788	8.602	0.001	0.057	0.573	0.449	0.287	0.259
	Sigmund & McCaffery	1	4.233×10^{-6}	1.088	8.193	0.049	0.142	0.869	0.449	0.287	0.213

4. Discussions

The nature of flooding brine with CO₂ and imbibition process afterwards makes it to be difficult to control. Very low viscosity of CO₂ and high density difference results in unfavourable mobility ratio. Viscous fingering seems to be an evitable process in such systems. Some former studies are done at conditions that lead to onset of viscous fingering in displacement tests. Peters and Flock (1981) have presented a dimensionless instability number to estimate the onset of viscous fingering in immiscible displacement processes:

$$I_{sc} = \frac{(M-1)(v-v_c)\mu_w D^2}{C^* \sigma k_{wor}} \quad (25)$$

In this equation I_{sc} is a dimensionless stability number, M is mobility ratio, v is superficial velocity and v_c is characteristics velocity, D is core diameter, C^* is wettability number determined experimentally and k_{wor} is permeability to water. They observed that dimensionless instability numbers below 13.56 is considered as flooding with presence of viscous fingering. In this study, according to the stability criteria for core flooding, during drainage test and injecting the non-wetting phase with very high viscosity ratio between fluids, the process should be done at very low displacement velocities (very low injection rates) to achieve a stable front. The problem with very low displacement rate is the creation of capillary end-effects. This means that the injection rate should be high enough to avoid capillary end-effect and low enough to avoid viscous fingering problems. This is a major challenge.

In order to overcome this challenge, results of the experiments with different rates are used to define correlations to fit to the parameters in the stabilized period. Figure 29 shows the effects of rate on the relative permeability end points values. By increasing the rate, these values increase and it start to stabilize in high injection rate. Following equation is fitted to the results:

$$k_r = a_1(1 - e^{-a_2 q}) \quad (26)$$

Where a_1 and a_2 are matching parameters. A similar method has been suggested by Bennion et al. (1991) in the case of rate dependent flooding experiments. Stabilized flow conditions are ideally obtained when considering infinite flow rates that lead to relative permeability values of $k_r = a_1$. The same procedure is used to fit the residual and initial saturation values. In this case the trend is decreasing at higher injection rates.

$$S_{wir} = a_1(1 + e^{-a_2 q}) \quad (27)$$

$$S_{CO_2r} = a_1(1 + e^{-a_2 q}) \quad (28)$$

Here S_{wir} is irreducible water saturation after drainage from curve fitting and S_{CO_2r} is the residual CO₂ saturation. Again, stabilized flow conditions are considered in the case of infinite flow rates that lead to $S_{wir} = a_1$, $S_{CO_2r} = a_1$. After fitting the correlations and determining the stabilized values, we have one set of relative permeability curves for each fluid set. The modifications show that the results are close to the highest injection rate tests. Curve fitting values from correlation 26 and 27 and 28 give the end points, while the curvatures of the final relative permeability models are obtained from the highest injection rate imbibition and drainage tests. Table 10 shows the fitting parameter and Figures 33 and 34 are relative permeabilities obtained after modification. In order to scale the results to the real storage reservoir conditions, the capillary number is

calculated for the experiments. Figure 32 shows the residual CO₂ saturation obtained from the experiment and is plotted against capillary number. Former simulation studies of Utsira brine formation of Sleipner and Viking formation (Canadian brine formation) revealed the range of capillary number using inter-block velocity in simulation model (Soroush et al., 2013).

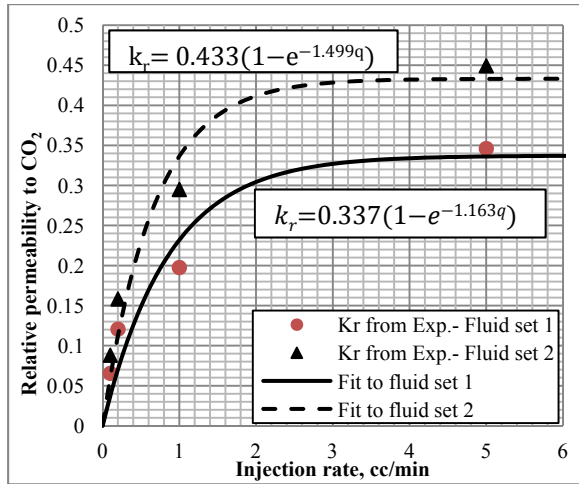


Figure 29. Relative permeability to CO₂, effect of imbibition rate and wettability

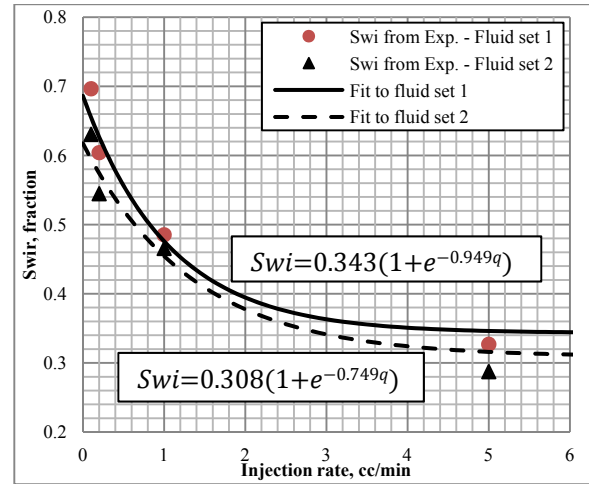


Figure 30. Swi, effect of drainage rate and wettability

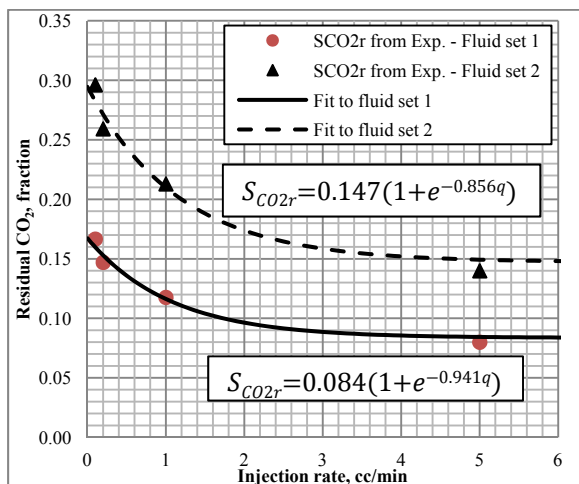


Figure 31. Residual CO₂, effect of imbibition rate and wettability

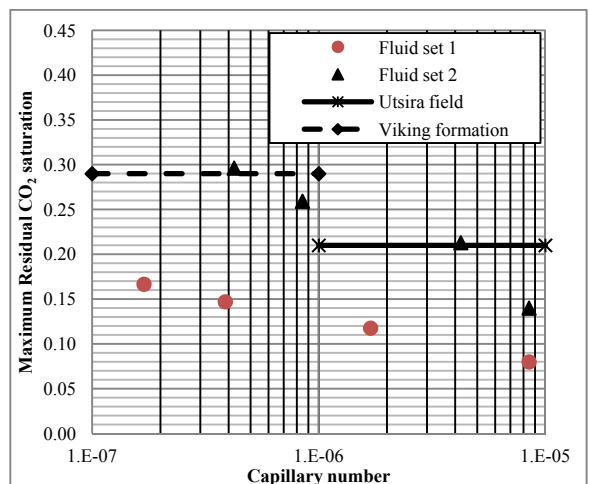


Figure 32. Residual CO₂ saturation effect of imbibition rate and wettability

Table 10. History matching data, eliminating effect of rate, modified relative permeability

Test type	Correlation	Fluid set	Nw	Ng	A	B	Krw(Sgi)	Krg(Swir)	Swir	Sgr
Drainage	Sigmund & McCaffery	1	5.765	8.680	0.816	0.245	1.000	0.337	0.343	0.000
	Corry	2	2.266	3.542	-	-	1.000	0.433	0.308	0.000
Imbibition	Sigmund & McCaffery	1	1.184	10.240	0.001	0.197	0.992	0.337	0.343	0.084
	Sigmund & McCaffery	2	1.088	8.193	0.049	0.142	0.869	0.433	0.308	0.147

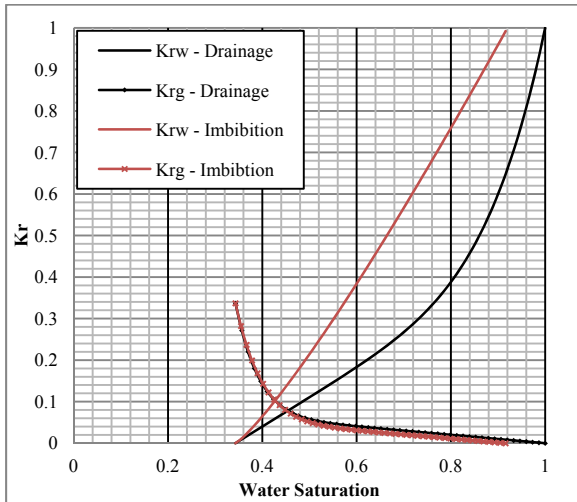


Figure 33. Modified relative permeability, fluid set 1

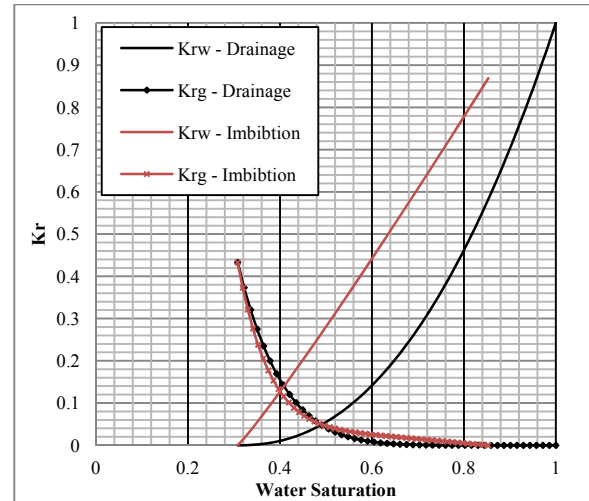


Figure 34. Modified relative permeability, fluid set 2

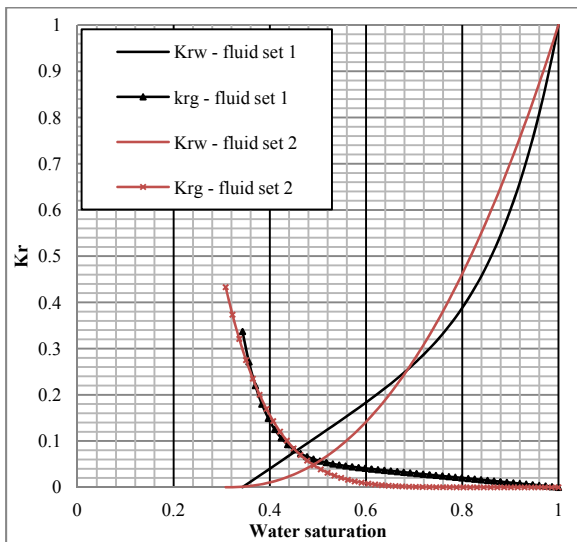


Figure 35. Drainage relative permeability, fluid set 1 and 2, effect of wettability

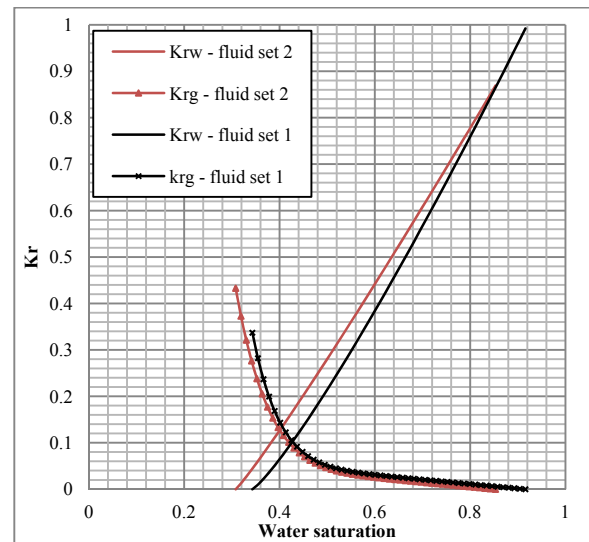


Figure 36. Imbibition relative permeability, fluid set 1 and 2, effect of wettability

In the experiments with fluid set 1 (higher wettability of wetting phase to the medium) residual CO₂ saturation is increased from 8% to 16.7% (8.7% grow) because of lowering the imbibition rate. On the other hand, in fluid set 2 (lower wettability of wetting phase) it is increased from 14% to 29.6% (15.6% grow). Using fluid set 2, the relative permeability to the CO₂ (non-wetting phase in the representative fluid) is increased by 9.6% while Sw_{ir} is decreased only by 3.5% because of rate effect.

By eliminating the effect of rate and comparing the results of the imbibition tests, the influence of wettability is analysed. Using fluid set 2, the relative permeability to the CO₂ (non-wetting phase in the representative fluid) is increased by 9.6% while Sw_{ir} is decreased only by 3.5%. Doing imbibition with fluid set 2 results in 12.3% decrease in relative permeability to water at the end point and CO₂ residual saturation increased from 8.4% to 14.7% (6.3% increase) and this is just because of different wettability characteristics of the system. Although the percentage of the change due to wettability is limited to this study, it can show the overall trend.

4.1 Validity of the Results

Relative permeability calculations are based on pressure drop readings from pressure transducer and volumetric and material balance and visual readings of the production. Although the pressure drops are in low ranges, the accuracy of the Fuji electronics pressure drop measurements that is used in this study is in the order of 0.01 mbar, which is acceptable. The production recording is double-checked by both volumetric and visual readings from the separator, and a minimum error is observed. 60 μm nylon filters are used at the chamber both ends to prevent glass beads production. Filter size has been optimized so that it is not being too fine to create errors in pressure drop and not too coarse to allow glass beads production. The pressure drop created by this filters is considered to be very small in comparison to the glass beads column pressure drop. There are also other laboratory conditions and simulations errors, but overall range of the error is acceptable.

5. Conclusions

In this study, laboratory experiments are carried out to investigate the effects of flooding rates in both drainage and imbibition processes in CO₂-brine systems. The wettability behaviour also created some interesting results in these systems. Results may be used in both new experimental activities (2D model set up in connection with this work) and in simulation studies. The following conclusions are offered:

- (1) Results of this study verify that using two sets of fluids representing the CO₂-brine systems in the reservoir can facilitate the research. Using a liquid-liquid system with the same density difference and viscosity ratio may not be exactly representative of the CO₂ storage at reservoir conditions; however, scaling the results shows that the designs are pretty close to the real conditions (figure 32).
- (2) Correlations are developed by fitting the residual CO₂ saturation and corresponding relative permeability in different rates and wettability conditions. Using these correlations, it is possible to estimate the CO₂ residual values in different aquifer influxes. This method is useful in obtaining estimations of CO₂ residuals in real cases.
- (3) The results show that in the case of less wettability of the wetting phase to the porous media, residual CO₂ trapping is more sensitive to the imbibition rate. This is clear from trend of CO₂ trapping volume versus capillary number in figure 32. For both sets of fluids, more CO₂ is trapped in lower capillary number (lower imbibition rate).
- (4) Comparison of the analysis of drainage and imbibition tests for two fluid sets shows the effect of wettability. In conclusion, using fluid set 2 (lower wettability of the wetting phase to the porous material) leads to increasing relative permeability to CO₂ and decreasing S_{wir} . Residual CO₂ saturation after imbibition process is increased because of using fluid set 2. Wettability affected the relative permeability values at the end points more than other parameters. The weakest effect is observed on the irreducible water saturation after drainage.

Acknowledgements

This publication has been produced with support from the BIGCCS Centre, performed under the Norwegian research program Centres for Environment-friendly Energy Research (FME). The authors acknowledge the following partners for their contributions: Conoco Phillips, Gassco, Shell, Statoil, TOTAL, GDF SUEZ and the Research Council of Norway (193816/S60). Special thanks to Erik Lindeberg, Torleif Holt, Øyvind Haave, Bård Bjørkvik, Szczepan Polak and Svein Arlid for invaluable technical supports, help and advice in SINTEF petroleum research.

References

- Bandara, U. C., Tartakovsky, A. M., & Palmer, J. (2011). Pore-scale study of capillary mechanism during CO₂ injection in geological formations. *International Journal of Greenhouse Gas Control* 5, 1566-1577. <http://dx.doi.org/10.1016/j.ijggc.2011.08.014>
- Bennion, B., & Bachu, S. (2005). Relative permeability characteristics for supercritical CO₂ displacing water in variety of potential sequestration zones in the western Canada sedimentary basin. SPE 95547, *SPE annual technical conference, Dallas, Texas, US*. <http://dx.doi.org/10.2118/95547-MS>
- Bennion, B., & Bachu, S. (2008). Drainage and imbibition relative permeability relationships for supercritical CO₂/brine and H₂S/brine systems in intergranular sandstone, carbonate, shale, and anhydrite rocks. *SPE Reservoir Evaluation & Engineering*, 11(3), 487-496. <http://dx.doi.org/10.2118/99326-PA>
- Bennion, B., & Thomas, F. B. (1991). Recent improvement in experimental and analytical techniques for determination of relative permeability from unsteady state flow experiments. Prepared for presentation at SPE 10th Technical conference in Port of Spain, Trinidad. Retrieved from

- http://www.weatherfordlabs.com/media/34746/recent_improvements_in_experimental-rel_perm.pdf
- Burdine, N. T. (1953). Relative permeability calculations from pore size distribution data. *Journal of Petroleum Technology*, 5(3), 71-78. <http://dx.doi.org/10.2118/225-G>
- Carlson, F. M. (1981). Simulation of relative permeability hysteresis to the non-wetting phase. SPE10157-MS, *Soc. of Pet. Eng., Richardson, TX*. <http://dx.doi.org/10.2118/10157-MS>
- Chiquet, P., Daridon, J. L., Broseta, D., & Thibeau, S. (2007). CO₂/water interfacial tensions under pressure and temperature conditions of CO₂ geological storage. *Energy Conversion and Management*, 48(3), 736-744. <http://dx.doi.org/10.1016/j.enconman.2006.09.011>
- Chierici, G. (1984). Novel relations for drainage and imbibition relative permeabilities. *Old SPE Journal*, 24(3), 275-276. <http://dx.doi.org/10.2118/10165-PA>
- Corey, A. T. (1954). The interrelation between gas and oil relative permeabilities. *Prod.*, 19(1), 38-41.
- Gupta, S., & Trushenski, S. (1979). Micellar flooding-compositional effects on oil displacement. *Old SPE Journal*, 19(2), 116-128. <http://dx.doi.org/10.2118/7063-PA>
- Hebach, A., Oberhof, A., Dahmen, N., Kögel, A., Ederer, H., & Dinjus, E. (2002). Interfacial tension at elevated pressures measurements and correlations in the water+ carbon dioxide system. *Journal of Chemical & Engineering Data*, 47(6), 1540-1546. <http://dx.doi.org/10.1021/je025569p>
- Honarpour, M., Koederitz, L., & Herbert, H. A. (1986). *Relative permeability of petroleum reservoirs*. C.R.C Press Inc.
- Iffly, R., Rousselet, D. C., & Vermeulen, J. L. (1972, October). Fundamental study of imbibition in fissured oil fields. In *Fall Meeting of the Society of Petroleum Engineers of AIME*. <http://dx.doi.org/10.2118/4102-MS>
- Johnson, E. F., Bossler, D. P., & Naumann, V. O. (1959). Calculation of relative permeability from displacement experiments. *Trans. AIME*, 216, 370-372.
- Kaviany, M. (1995). *Principles of heat transfer in porous media* (2nd Ed.). New York: Springer.
- Killough, J. E. (1976). Reservoir simulation with history-dependent saturation functions. *Old SPE Journal*, 16(1), 37-48. <http://dx.doi.org/10.2118/5106-PA>
- Kleppe, J., Delaplace, P., Lenormand, R., Hamon, G., & Chaput, E. (1997, October). Representation of capillary pressure hysteresis in reservoir simulation. In *SPE Annual Technical Conference and Exhibition*. <http://dx.doi.org/10.2118/38899-MS>
- Krause, M., Perrin, J. C., & Benson S. M. (2011). Recent progress in predicting permeability distribution for history matching core flooding experiments. *Energy Procedia*, 4, 4354-4361. <http://dx.doi.org/10.1016/j.egypro.2011.02.387>
- Krever, S. C. M., Pini, R., Zou, L., & Benson, S. M. (2011). Relative permeability and trapping of CO₂ and water in sandstone rocks at reservoir conditions. *Water resources research*, 48. <http://dx.doi.org/10.1029/2011WR010859>
- Kua, C. W., Perrin, J. C., & Benson S. M. (2011). Simulation studies of effects of flow rate and small scale heterogeneity on multiphase flow of CO₂ and brine. *Energy Procedia* 4, 4516-4523. <http://dx.doi.org/10.1016/j.egypro.2011.02.408>
- LAND, C. (1971). Comparison of calculated with experimental imbibition relative permeability. *Old SPE Journal*, 11(4), 419-425. <http://dx.doi.org/10.2118/3360-PA>
- Lomeland, F., Ebeltoft, E., & Thomas, W. H. (2005, August). A new versatile relative permeability correlation. In *international symposium of the society of core analysts held in Toronto, Canada*. Retrieved from <http://www.ri.reslab.no/sendra-papers.aspx>
- Nordbotten, J. M., Celia, M. A., & Bachu, S. (2005). Injection and storage of CO₂ in deep saline aquifers: Analytical solution for CO₂ plume evolution during injection. *Transport in Porous media*, 58(3), 339-360. <http://dx.doi.org/10.1007/s11242-004-0670-9>
- Perrin, J. C., & Benson, S. (2010). An experimental study on the influence of sub-core scale heterogeneities on CO₂ distribution in reservoir rocks. *Transport in porous media*, 82(1), 93-109. <http://dx.doi.org/10.1007/s11242-009-9426-x>
- Peters, E., & Flock, D. (1981). The onset of instability during two-phase immiscible displacement in porous

- media. *Old SPE Journal*, 21(2), 249-258. <http://dx.doi.org/10.2118/8371-PA>
- Pini, R., Krevor, S. C. M., & Benson, S. M. (2012). Capillary pressure and heterogeneity for the CO₂-brine system in sandstone rocks at reservoir conditions. *Advances in Water Resources* 38, 48-59. <http://dx.doi.org/10.1016/j.advwatres.2011.12.007>
- Rumpf, H., & Gupte, A. R. (1975). The influence of porosity and grain size distribution on the permeability equation of porous flow. *NASA STI/Recon Technical Report N*, 75, 30484.
- Schlumberger eclipse technical description. (2012). Retrieved from <http://www.slb.com>
- Sendra user guide. (2012). Retrieved from <http://www.sendra.no>
- Sigmund, P. M., & McCaffery, F. G. (1979). An Improved Unsteady-State Procedure for Determining the Relative-Permeability Characteristics of Heterogeneous Porous Media (includes associated papers 8028 and 8777). *Old SPE Journal*, 19(1), 15-28. <http://dx.doi.org/10.2118/6720-PA>
- Soroush, M., Wessel-Berg, D., & Kleppe J. (2013), Effects of wetting behaviour on residual trapping in CO₂-brine systems. 165334-MS, *SPE Western Regional & AAPG Pacific Section Meeting, Joint Technical Conference, Monterey, CA, USA*. <http://dx.doi.org/10.2118/165334-MS>
- Spiteri, E., Juanes, R., Blunt, M., & Orr, F. (2008). A new model of trapping and relative permeability hysteresis for all wettability characteristics. *Spe Journal*, 13(3), 277-288. <http://dx.doi.org/10.2118/96448-PA>
- Suekane, T., Zhou, N., Hosokawa, T., & Matsumoto, T. (2010). Direct observation of trapped gas bubbles by capillarity in sandy porous media. *Transport in porous media*, 82(1), 111-122. <http://dx.doi.org/10.1007/s11242-009-9439-5>
- Wang, J., Dong, M., & Asghari, K. (2006, April). Effect of Oil Viscosity on Heavy Oil-Water Relative Permeability Curves. In *SPE/DOE Symposium on Improved Oil Recovery*. <http://dx.doi.org/10.2118/99763-M>
- Wessel-Berg, D., Kleppe, J., & Soroush, M. (2013, June). Investigating Residual Trapping Mechanism in CO₂ Storage in the Brine through Analytical and Numerical Simulation Methods. In *75th EAGE Conference & Exhibition incorporating SPE EUROPEC 2013*. <http://dx.doi.org/10.2118/164808-MS>

Copyrights

Copyright for this article is retained by the author(s), with first publication rights granted to the journal.

This is an open-access article distributed under the terms and conditions of the Creative Commons Attribution license (<http://creativecommons.org/licenses/by/3.0/>).